

Gamma-Irradiation Improves the Photocatalytic Activity of Fe/TiO₂ for Photocatalytic Degradation of 2-Chlorophenol

Karim. R. Diab^{*1} M. M. Doheim² Sawsan A. Mahmoud² S. A. Shama³ H. A. El-Boohy⁴

1.Desert Research Center (DRC), Cairo, Egypt

2.Egyptian Petroleum Research Institute (EPRI), Cairo, Egypt

3.Department of Chemistry Faculty of Science, Benha University, Benha, Egypt

4.National Center for Radiation Research and Technology (NCRRT), Cairo, Egypt

Abstract

The Fe doped TiO₂ abbreviated here as (Fe₃) were prepared by sol-gel method. Upon doping FeTiO₃ nano-composite was formed. The prepared sample was irradiated by different dosage of γ -irradiated (0.2, 0.4, 0.8 and 1.6 MGy). The irradiated samples which abbreviated as (0.2, 0.4, 0.8 and 1.6 MGy) and non-irradiated sample which abbreviated as (Fe₃) were characterized by X-Ray Diffraction (XRD), Surface analysis, Scanning Electron Microscopy (SEM), Transmission Electron Microscopy (TEM), Temperature Programmed Desorption (NH₃-TPD), Raman Spectroscopy, and UV-Vis absorption. The results show that γ -irradiation not only improves the morphological and structural changes of irradiated samples, but also extended its absorption edge to the visible light region. The photocatalytic activity of the samples were tested for the photocatalytic degradation of 2-chlorophenol under simulated solar light irradiation. The photocatalytic activity of the irradiated sample using 1.6 MGy was higher than the other irradiated and non-irradiated samples. The photo-intermediate product was also studied.

Keywords: Photocatalysis, TiO₂, 2-chlorophenol, photocatalytic degradation, Gamma-irradiation.

1. Introduction

Phenolic compounds constitute an important family of contaminants of wastewater produced by chemical, petrochemical or biotechnological industries. As they have high toxicity and a carcinogenic character, they have caused damage and threat to the environment and human health. Current water treatment methods, which can be achieved using conventional water treatment technologies, are often not fully acceptable when waste water include significant amounts of compounds having toxic effect on the microorganism that responsible for biological degradation of the organic waste [1,2], as phenolic type pollutants [2,3]. Among promising technologies to accomplish this task, novel and efficient advanced oxidation techniques based on catalytic or chemical photo oxidation are emerging as a promising alternative [4]. For this reason, heterogeneous photocatalysis can be applied to remove pollutants existing in the wastewater.

TiO₂ has been widely used as photocatalyst and catalyst support for variety of applications [5, 6]. In particular, the TiO₂ (anatase) has been extensively used for several photo catalytic reactions for the removal of many organic pollutants from waste water [7–9]. But, its photocatalytic properties can be restricted by hole-electron recombination or by its relatively large band gap [10]. Though, there are trials to reduce electron-hole recombination rates and increase photo-catalyst efficiency. A common method consists in doping of TiO₂ with transition metal cations while keeping a good control of the primary particle size to reach nano-scale sizes of the catalysts [11]. Fe is considered an interesting dopant of TiO₂, because it can act as shallow traps in the titania lattice.

Ionizing radiations and doping with certain metal oxides brought about significant changes in the chemistry of surface of most of solid catalysts.

Modification in textural, structural, electrical, thermal, and magnetic properties of large variety of solids due to irradiation with ionizing one such as γ -rays have been reported [12]. These changes are commonly cause many modification in surface, catalytic, and thermal properties of irradiated materials.

Ionizing radiation was found to be able to change catalytic activities and surface oxidative abilities of various mixed oxides [13]. Irradiating CuO-ZnO/TiO₂ and Co₃O₄/MgO with γ -rays increases its activity towards alcohol conversion reaction using micro pulse technique [14] and change the catalytic activity of Na₂OMn₂O₃/Al₂O₃, Co₃O₄/Al₂O₃ and Mn₂O₃-MnO₂ systems towards the same reaction [15-16].

It is noticed that γ -irradiation has been reported to achieve increase in the specific surface areas and the catalytic activities of certain catalytic systems depending on the nature of the irradiated solid, the dose of γ -rays and the nature of catalyzed reaction

The present work is devoted to study the effect of different doses of γ -irradiation on the surface and catalytic properties of Fe-TiO₂ system.

2-Experimental

2.1. Catalyst preparation

Pure Titanium dioxide nano-particles were prepared by the sol-gel method using titanium tetraisopropoxid as titanium precursor. 10 ml titanium alkoxide was mixed with 40 ml 2-propanol with constant stirring. This mixture was then added drop wise to a solution consisting of 10 ml distilled water and 10 ml 2-propanol in alkaline medium at pH = 9 adjusted using ammonium hydroxide. A yellowish gel was formed. The formed gel was stirred for 1 hour. The as prepared precipitate was dried at 105 °C for four hours. Calcination of the synthesized material was carried out in air at 500 °C for four hours.

Iron doped titanium oxide was prepared by the same procedure mentioned above. 80 ml Iron acetylacetonate containing 3 wt% of Fe³⁺ was dissolving in 2-propanol. The dissolved Iron acetylacetonate was added drop wise to 10 ml titanium isopropoxide in 40 ml 2-propanol. The pH of the solution was adjusted at 9 by NH₄OH. The produced yellowish gel was stirred for 1 hour. The as prepared precipitate was dried at 105 °C for four hours. Calcination of the synthesized material was carried out in air at 500 °C for four hours.

The prepared iron doped titanium oxide Fe/TiO₂ abbreviated as (Fe 3) was exposed to different doses of γ -rays namely 0.2, 0.4, 0.8 and 1.6 MGy. The irradiated samples were kept in sealed tubes for 3 weeks before conducting the different measurements to avoid any temporary effect that may be induced by γ -irradiation. The samples were irradiated with the Co⁶⁰ Indian research irradiator gamma chamber with activity 9100 curies at a dose rate ranging from 4 to 4.4 kGy/h. The irradiation chamber was constructed by the National Center for Radiation Research and Technology (NCRRT), Atomic Energy Authority of Egypt (AEAE) Cairo.

2.2. Catalyst characterization

- XRD analysis was performed using a PAN analytical X'Pert PRO diffractometer in reflection mode using CuK α radiation ($\lambda = 0.1542$ nm) at 40 Kv and 40 mA, over the scan range of 2θ between 20 and 80 at 295 K, in order to identify the phase present.
- Transmission Electron Microscopy (TEM) studies were carried out using a JEOL JEM-2100 electron microscope operating at 120 kV.
- BET surface area of the synthesized samples were measured on Quantachrome NOVA 2000 system (USA), at -196 °C after degassing at 300 °C and 10⁻⁵ mmHg for 4 h.
- Scanning Electron Microscopy (SEM) investigation was performed by JEOL JEM 3500 electron microscope to confirm the surface morphology of the prepared materials.
- Energy Dispersive X-ray Spectroscopy (EDX) is a chemical microanalysis technique used in conjunction with SEM to characterize the elemental composition of the prepared material.
- UV-Vis absorption spectrum was measured at room temperature in the range from 200 to 2500 nm using a Scan UV-Vis spectrophotometer (type JASCO corp., V-570, Rel-00, Japan).
- Raman spectroscopy is carried out using Bruker SENTERRA dispersive Raman microscope ($\lambda = 532$ nm).
- Temperature Programmed Desorption (TPD). TPD analysis was conducting using a BELCAT-B Temperature Programmed Desorption instrument model BELCAT-B serial No CAT-146 BEL. Japan.INC

2.3. Photocatalytic activity measurement

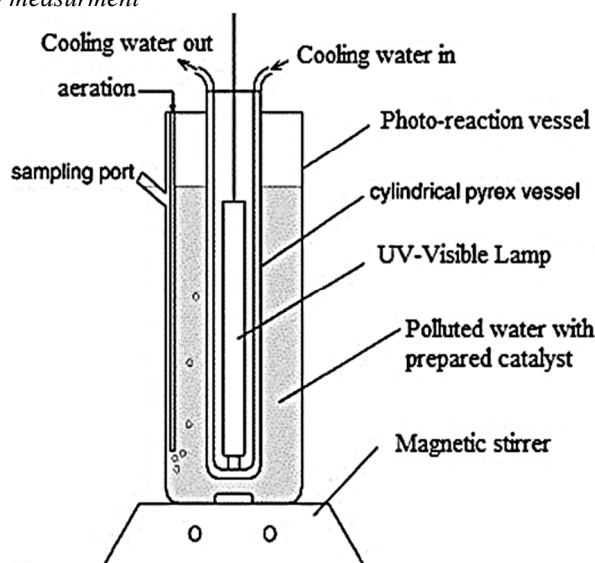


Figure1. Schematic diagram of photo-reactor.

Quartz batch photoreactor of cylindrical shape (Figure 1), containing 500 ml of aqueous suspension, was

used for performing the reactivity experiments. A magnetic stirrer guaranteed a satisfactory suspension of the photocatalyst and the uniformity of the reacting mixture. UV-vis lamp (365 nm) was axially immersed within the photoreactor and it was cooled by water circulating through a quartz thimble; the temperature of the suspension was about 300 K. The initial concentration of 2-CP was 100 ppm. The polluted water was aerated using a bubble distributor. The experiments were performed at room temperature and the pH of the reaction mixture was kept at 5.5. Prior irradiation, the slurry was aerated for 10 min at dark to reach adsorption equilibrium followed by UV-vis irradiation. Adequate aliquots (5 cm^3) of the sample were withdrawn after periodic interval of irradiation and analyzed after filtration using: (a) HPLC PerkinElmer series 200 provided with photodiode array detector at 280 nm wavelength and C8 column ($4.6 \text{ cm} \times 25 \text{ cm}$). The mobile phase was acetonitrile/water in the ratio of 60:40 (v/v) with a flow rate of 1 ml/min. (b) Ion chromatograph (Dionex-pac) was used to determine the concentration of chloride and acetate ions.

3. Results and Discussion

3.1. XRD

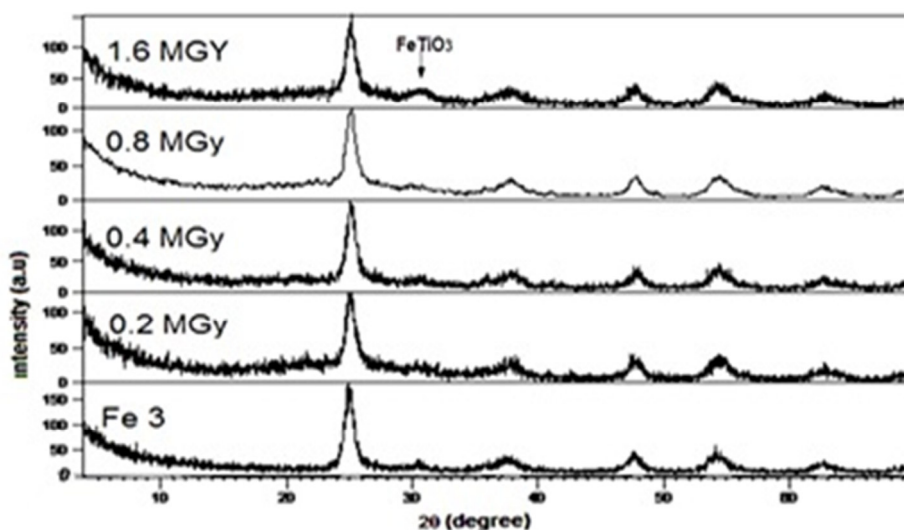


Figure 2: Cumulative XRD diffractograms of the non-irradiated $\text{Fe}_2\text{O}_3/\text{TiO}_2$ (Fe_3) and irradiated samples (0.2, 0.4, 0.8 and 1.6 MGy).

Figure 2 shows the XRD patterns of iron doped TiO_2 (Fe_3) and irradiated samples, it can be seen that, Fe/TiO_2 (Fe_3) represents a sharp peak at $2\theta = 25.23^\circ$ corresponds to anatase phase. Upon Fe doping, the major peak of anatase phase appear to be the same but the intensity was reduced. the appearance of a new peak correspond to FeTiO_3 at $2\theta = 32.529^\circ$ was also detected. In addition the peak broadening can be attributed to the expansion of the cell and decrease in the crystallite size (Table 1). The expansion of the cell could be recognized due to significant difference between ionic radii of the dopant and the host ions (Fe^{3+} : 0.069 \AA and Ti^{4+} : 0.745 \AA , with a coordination number of 6).

No peaks corresponding to iron oxide is detected due to the highly dispersed iron species on the surface.

The diffraction peaks of the non-irradiated and irradiated samples with different dosage (0.2, 0.4, 0.8 and 1.6 MGy) are in anatase and a minor diffraction peak belong to ilmenite FeTiO_3 at ($2\theta = 32.529^\circ$) [17] and the diffraction peak become more broaden at (1.6MGy).

The crystallite sizes were calculated using Scherrer equation [18] after correction for instrumental broadening. [$D = K \lambda / (\beta \cos \theta)$] While D = is the mean particle diameter, K = is the Scherer constant (0.89), λ = is the wave length of the X- ray beam (1.5405 \AA), β = is the full width half maximum of the 101 anatase diffraction line and θ = is the diffraction line of the investigated phase.

Table 1: Effect of γ -irradiation on the crystallite size of the non-irradiated and irradiated samples.

Catalyst	crystallite size (nm)
$\text{TiO}_2\text{-Fe}_2\text{O}_3$ (Fe_3)	11
0.2 MGy	12.8
0.4 MGy	13.04
0.8 MGy	11.7
1.6 MGy	10

From Table1 we can conclude the following:

- The crystallite size of all the samples is detected in the range from 13.04 to 10 nm.
- γ -Irradiation of most samples investigated with small doses increases slightly the crystallite sizes of all

phases present then decreases it at higher doses this result is consistent with previous literature[19] It is clearly shown for the irradiated Fe-TiO₂ with dose(1.6 MGY) that the peak of FeTiO₃ become more broaden with increasing the dose of gamma irradiation, this could be attributed to the more dispersion and uniform distribution of iron composite on the surface of the catalyst . The photocatalytic activity of (1.6 MGY) was improved with uniform distribution of FeTiO₃ phase, which was explained by the good photo-absorbance capacity and by the two-step electron transfer model.

3.2. UV–Visible absorption measurements

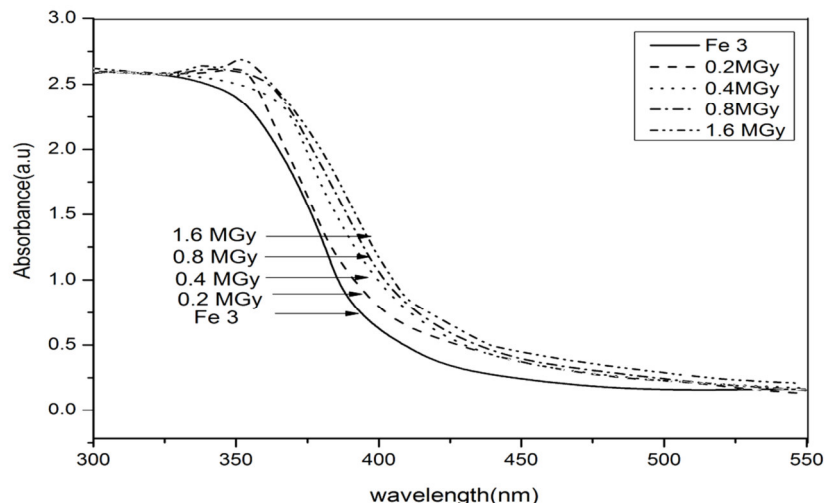


Figure 3: UV–Visible spectra of the non- irradiated(Fe3) and irradiated samples (0.2, 0.4, 0.8 and 1.6 MGy). UV–Visible spectra of the non-irradiated (Fe3) and irradiated samples with dose 0.2, 0.4, 0.8 and 1.6 MGy are shown in Figure 3. The absorption edge is found to shift in a systematic manner to longer wavelength with increasing the dose of γ irradiation in Fe-TiO₂ in comparison to non irradiated sample.

From these spectra, the band gap energy (E_g) value of the samples was calculated using equation[20]:

$$\alpha h\nu = A (h\nu - E_g)n/2 \dots\dots\dots (1)$$

Where α is the absorption coefficient, $h\nu$ is the photon energy, $n \sim 1$ for direct transition between bands and E_g is the energy of the band gap. The simplification of the above equation into the formula:

$$E_g = 1240.82/\lambda \dots\dots\dots (2)$$

Where λ is the absorption band edge wavelength (nm).

For practical purposes, the energy band gap value was calculated by extrapolation of the absorption band to the x-axis. The band gap value of the samples is reported in Table 2.

Table 2: Band gap value of the non-irradiated and irradiated samples.

Catalyst	Band gap (eV)
TiO ₂ -Fe ₂ O ₃ (Fe 3)	2.64
0.2 MGy	2.63
0.4 MGy	2.61
0.8 MGy	2.59
1.6 MGy	2.51

This data clearly reveal that the band gap energy of doped TiO₂ samples decrease with increasing the dose of γ -irradiation. With increase the dose of γ - irradiation in the Fe- TiO₂ lattice, the band gap is lowered to 2.63eV for (0.2 MGy), further reduced to 2.51eV for (1.6 MGy).

This absorption enhancement with decrease in band gap in the visible region could be attributed to the effect of γ -irradiation on iron and iron composite (FeTiO₃) which became more dispersed and well distributed on the surface of the

3.3. Raman spectroscopy

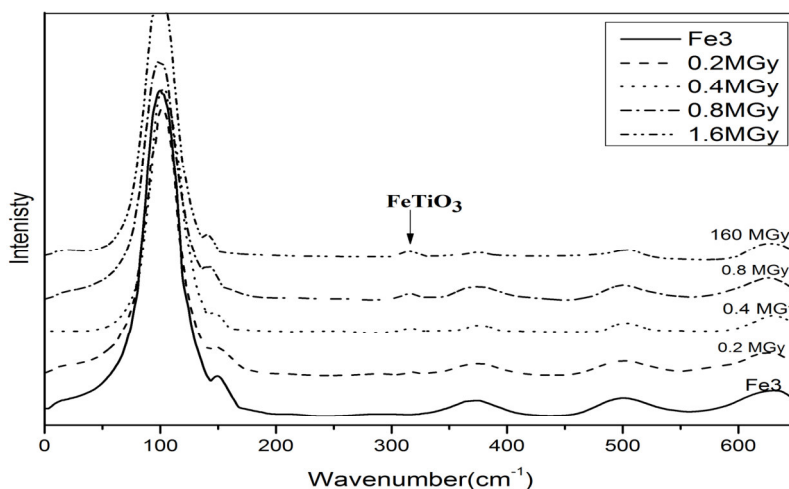


Figure 4: Raman spectra of the non irradiated and irradiated samples.

Figure 4 shows the Raman spectra of different samples. Raman peak at about 146 cm^{-1} is the strongest of all the observed bands, which is observed for all the samples, which is attributed to the main E_g anatase vibration mode. Moreover, vibration peaks at 199 cm^{-1} (E_g , weak), 399 cm^{-1} (B_{1g}), 516 cm^{-1} (A_{1g}) and 640 cm^{-1} (E_g) are presented in the spectra for all samples, which indicates that anatase TiO_2 crystalline are the predominant species [21].

Furthermore, there are Raman lines corresponding to FeTiO_3 at 330 cm^{-1} observed in irradiated catalysts with dose (0.2, 0.4, 0.8, and 1.6 MGy) and the intensity of peak most increase in (1.6MGy), which is consistent with the results of XRD patterns.

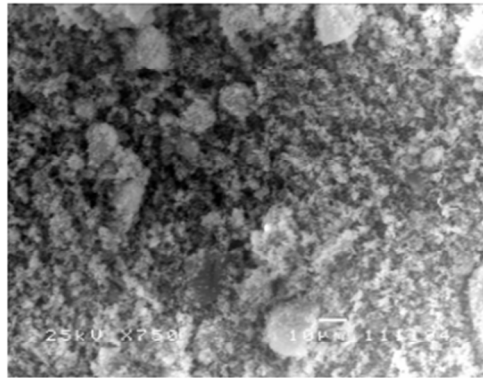
But the FeTiO_3 in non-irradiated (Fe 3) seems to have exhibited no prominent Raman bands, this result in Raman is contrary with XRD and these maybe due to the fact that this new band has very low intensity relatively to the characteristic bands of TiO_2 (this result is consistent with the literature[22])

The appearance of FeTiO_3 band in irradiated catalysts could be attributed to the effect of γ -irradiation on the high distribution of FeTiO_3 which resulting in prominent Raman bands.

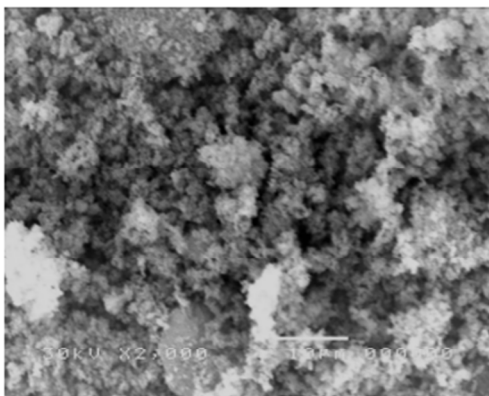
3.4. SEM

Figure 5 shows The SEM micrographs of the irradiated and non irradiated samples. It can be seen that the non irradiated sample is different in size from those of irradiated with dose (0.2, 0.4, 0.8, 1.6). In general, the higher dose of γ -irradiation (1.6 MGY) consists of nano-sized primary particles with spherical shape, whereas non irradiated sample consists of relatively larger particle size.

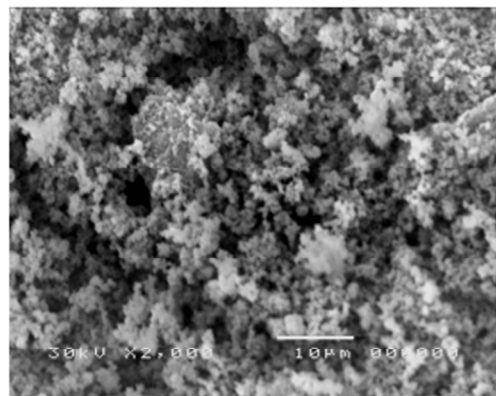
SEM investigations gave evidence that, the agglomeration decreased with increase the dose of γ rays. There is no change in the morphology of irradiated samples after irradiation with γ -rays that might be attributed to the iron oxides are well dispersed within the TiO_2 phase.



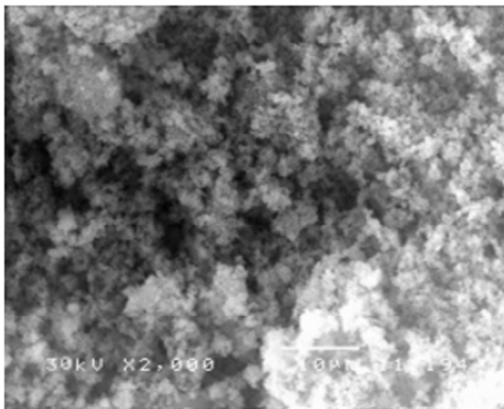
$Fe_2O_3/TiO_2(Fe_3)$



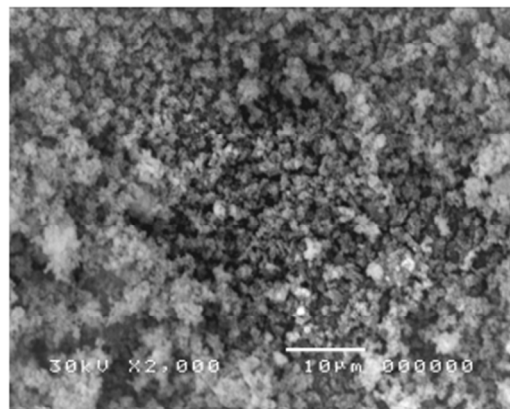
0.2MGy



0.4MGy



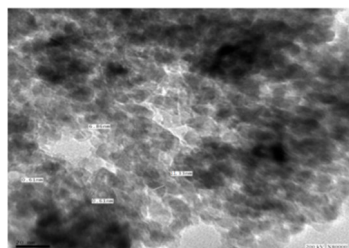
0.8 MGy



1.6 MGy

Figure 5: SEM Micrographs of the non irradiated and irradiated samples

3.5. TEM



Fe₂O₃/TiO₂ (Fe₃)

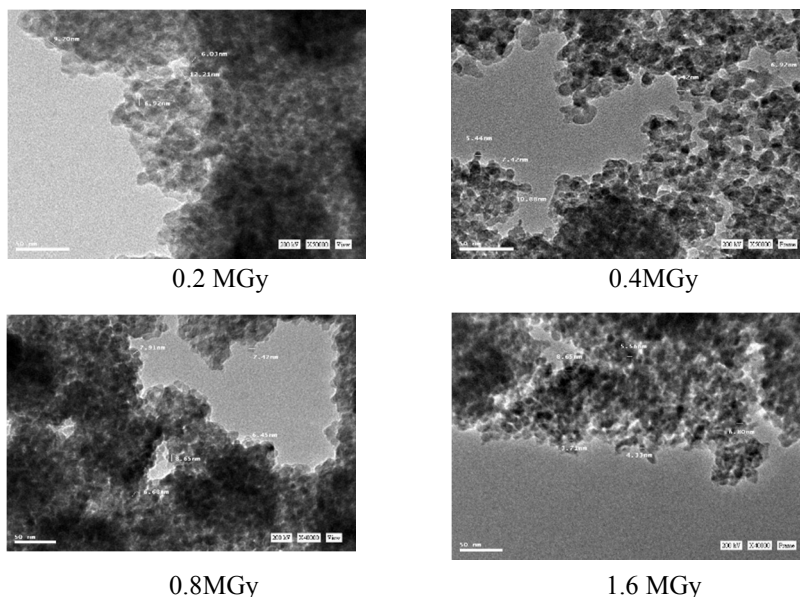


Figure 6: TEM Micrographs of the non irradiated and irradiated samples

Figure 6 shows the transmission electron micrographs (TEM) of the non irradiated and irradiated samples. It can be seen that the sizes of non irradiated particles ranged from 11.33 to 9 nm. However, the sizes of irradiated particles with dose (1.6MGy) ranged from 8.7 to 6 nm. It is evident from this micrograph that the nanoparticles become smaller and smaller at the high dose of γ -irradiation, which is in close agreement with average crystallite size obtained from XRD studies. This is easy to be understood because γ -Irradiation has been reported to decrease the crystallite size [23].

TEM investigations gave evidence of no segregated secondary phases of iron oxides and supports homogeneously distribution in the TiO₂ matrix which is consistent with the results of XRD patterns and SEM micrographs.

3.6. Surface area measurement

The surface characteristics including the surface areas (S_{BET}), total pore volume and Average pore size were calculated for non-irradiated and irradiated samples and the results obtained are listed in Table 4.

Table 3 : S_{BET} surface of the non-irradiated and irradiated samples.

γ -Irradiation dose (MGy)	BET (m ² /g)	Total pore volume (cc/g)	Average pore size (nm)
0.0	42.93	0.021	19.95
0.2	52.11	0.039	19.06
0.4	57.88	0.028	19.95
0.8	66.55	0.020	21.82
1.6	74.43	0.036	19.72

Table 3 shows the following:

- (i) The increase of the dose of γ -irradiation of investigated irradiated samples resulted in a significant increase in the values of their surface area measurements in comparison with non-irradiated catalyst.
- (ii) The maximum increase in the BET and total pore volume are showed in the high dose of γ -irradiated catalyst (1.6MGy)

The significant increase in the S_{BET} and pore volume of sample that exposed γ -irradiation with dose (1.6MGy)

could be attributed to both splitting of particles of the irradiated solids and creation of new pores [23].

3.7. NH₃-TPD

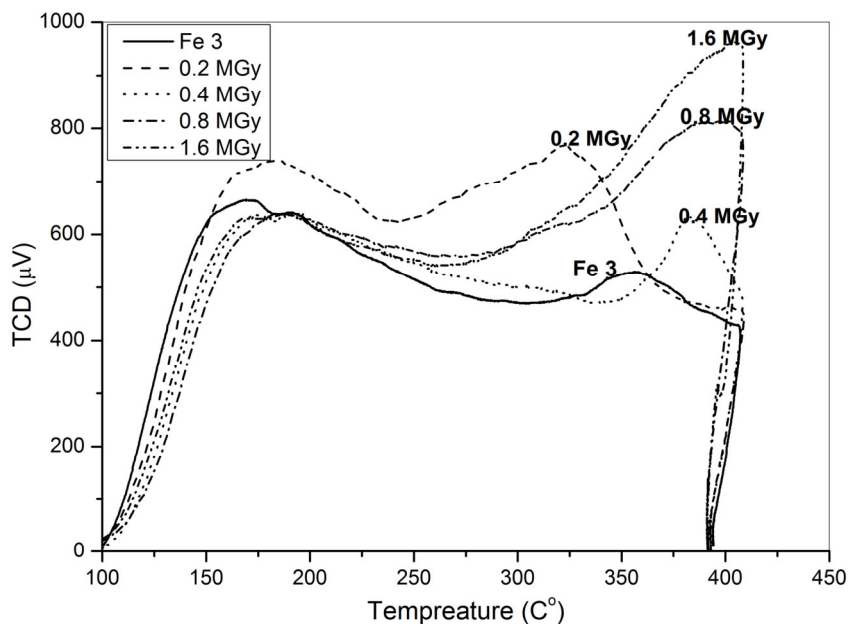


Figure 7. NH₃-TPD profile of the non-irradiated and irradiated samples.

Figure 7 shows the NH₃-TPD profiles. This Figure shows two parts: one that appears at temperatures between 125 and 225 °C, which is related to physical adsorption, and the other appears at temperatures between 250 and 400 °C. In general, the low and high temperature peaks corresponded to the weak and strong acid sites, respectively.

It can be seen that with increasing the dose of γ -Irradiation, the intensity of surface acidity and the amount of surface acid sites increases. This finding indicates that the new acid sites on the TiO₂ photo-catalyst framework are generated by the increase of γ -Irradiation dose. Therefore, these acid sites can partially affect the process of 2-chlorophenol removal.

The observed increase in the intensity of surface acidity and the amount of surface acid sites at high dose of γ -Irradiation (1.6 MGy) could be attributed to creation of new pores by γ -Irradiation.

3.8. Adsorption and photocatalytic degradation

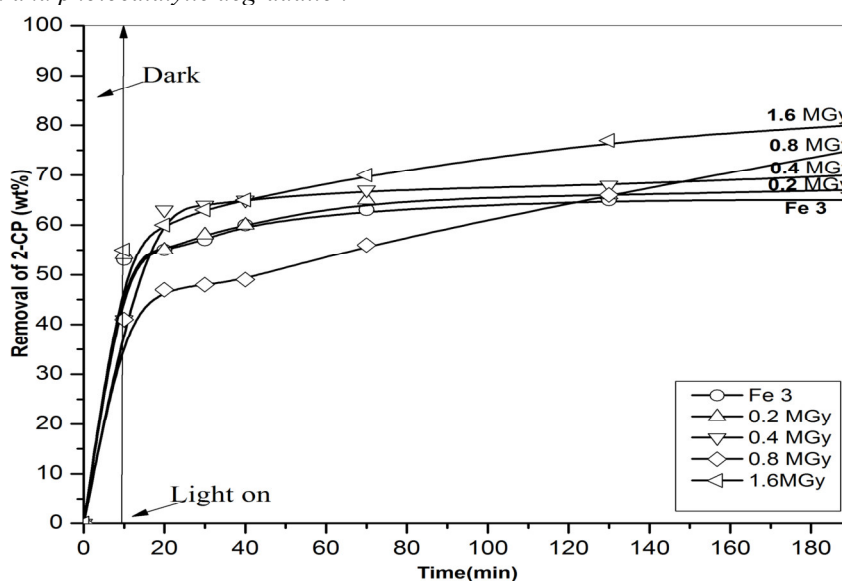


Figure 8: Effect of the reaction time on the photo degradation of 2-chlorophenol from the polluted water.

Figure 8 shows that 1.6 MGy catalyst has better adsorption capability to 2-CP than the other irradiated samples in dark region (10 min). Upon using 1.6 MGy catalyst sample, 45% of the starting concentration of 2-

CP is adsorbed using 0.1 g/l catalyst dosage. While 35, 38, 40 and 42% of 2-CP are adsorbed on non-irradiated sample, 0.2, 0.4 and 0.8 MGY using the same catalyst weights. It is well known that the adsorption of organics from water on adsorbents is not only influenced by the surface area but also affected by the hydrophobicity or the polarity of adsorbents. The adsorption capacity of samples increases with increasing the dosages of irradiation due to increase in the applied area for the adsorption. The decrease in the adsorption could be attributed to the high concentration of the chloride ion produced in water during the adsorption process. However, the presence of chloride ion compete with the 2-CP in the adsorption process on the surface of the catalyst and hence retard the process [24]. The adsorption of chloride ion on the TiO₂ surface most probably changes some of the surface characteristics of TiO₂ nanoparticles due to the change of the ζ -potential of TiO₂ in the aqueous solution [25].

Figure 8 shows the effect of the different irradiation dosages on 2-CP degradation. The photoactivity of the samples was conducted under the same conditions after the adsorption equilibrium was achieved. The results show that the photocatalytic degradation increased with increasing the irradiation dose. The degradation reached a maximum value of 80% of the initiate concentration with dosage of 1.6 MGY after 180 min of irradiation of UV. However, the increase in the irradiation dose increases the degradation efficiency. The photodecomposition rates of pollutants are influenced by the active sites and the photo-absorption of the catalyst used. The high irradiation dosage for the catalyst decreases the rate of electron/hole pairs recombination and enhancing the degradation of the pollutants. Figure 8 also shows the effect of the irradiation dosage on 2-CP degradation. The photocatalytic degradation of all samples was carried out under the same condition. The degradation reached a maximum value of 80% of the initiate concentration with irradiation dosage of 1.6MGY. However, a further increase in the catalyst dosage slightly decreased the degradation efficiency. Moreover, the degradation rate decreased to 37% with catalyst dosage of 0.4g/l. 1.6MGY is most active than 0.2, 0.4, 0.8 and non-irradiated catalyst for the photo-decomposition of 2-CP. Only the high dose of γ -irradiation (1.6MGy) showed the highest photocatalytic activity, this increase in photocatalytic activity could be attributed to several reasons based on the textural and chemical properties of the prepared and irradiated samples:

The observed increase in their surface area, it has been reported that the main function of γ -irradiation of some catalytic solid systems took place via splitting of particles of the irradiated solids and fragmentation of catalyst's constituents [19].

The observed increasing in the intensity of surface acidity, the amount of surface acid sites and can be attributed to the creation of a new pores on the surface of the catalyst

The enhancement of the activity of irradiated Fe/TiO₂ catalysts in comparison to non-irradiated (according XRD), may be due to different content of FeTiO₃ and highly homogeneous dispersion of iron species on surface. Especially, irradiated FeTiO₃ nano-composite improves the photocatalytic activity. This may be also due to FeTiO₃ has a good light absorbance and favorable photo-excited electron-hole separation characters.

Additionally, there are many other factors influencing catalytic activity; (1) Tsai and Cheng [26] reported that the high density of OH groups hinder the electron hole recombination consequently increase the photocatalytic degradation. The HO- on the surface is controlled the surface hydrophilicity. 1.6MGY which is more hydrophilic catalyst facilitates the adsorption of polar and hydrophilic pollutants as reported by Hsien *et al.* [27] (2) Abdel-Aal and Mahmoud [28] suggested that there is a clear relationship between substrate adsorption capacity and the photocatalytic activity. The more adsorbed pollutant on the catalyst surface, the faster the degradation. (3) Cho *et al.*, [29] assumed that intermediate generated during the 2-CP or 4-CP degradation continue to initiate a further degradation, and no toxic substances accumulate. (4) Xu *et al.* [30] and Gerischer [31] studied the effect of particle size on the photocatalytic efficiency of TiO₂. Both researchers concluded that the photocatalytic reactivity of TiO₂ increases with decrease in particle size. The obtained data of our study was agreed with these reported results.

3.9. Photo- intermediate products

Catechol (CT) is the only aromatic intermediate identified by HPLC during the degradation process of 2-CP [32]. Figure 9 shows the formation of catechol using non-irradiated and irradiated sample with different doses. It shows that the formation of catechol starts very early to reach a max of 15, 13 and 12 ppm for the non-irradiated sample (Fe₃), 0.2 and 0.4 MGY, respectively. The concentration then very slightly decreases to reach 12, 10 and 7.5 ppm for the non-irradiated sample(Fe₃), 0.2 and 0.4 MGY, respectively after 180 min of irradiation. The presence of CT in the aqueous phase compete with 2-CP in the adsorption on the surface of the catalyst and hence decrease the photocatalytic degradation of 2-CP. Figure 9 also shows that as the irradiation dosage increase, the formation of CT decreases.

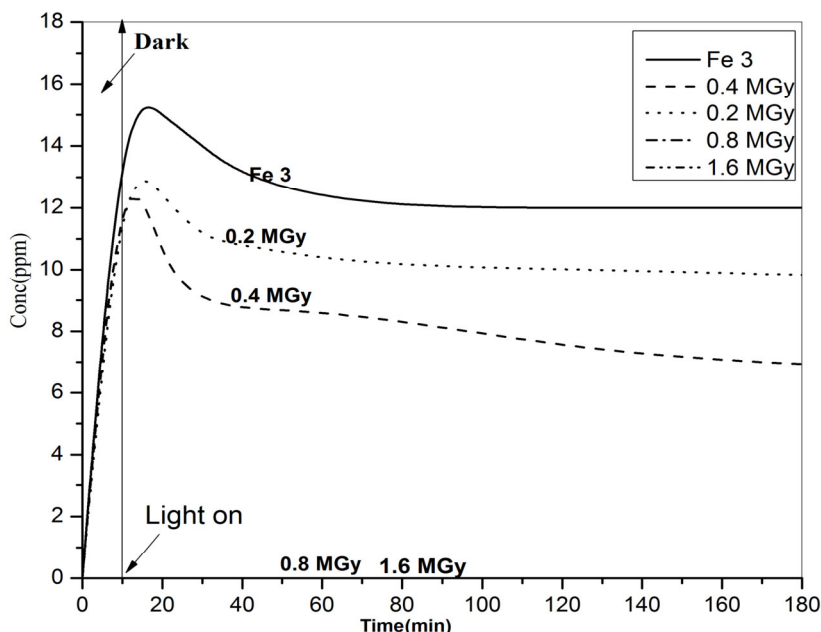


Figure 9: Effect of the reaction time on the production of Catechol in the Photo degradation of 2-chlorophenol from the polluted water.

CT is known to be strongly adsorbed on the catalyst surface, forming long wavelength absorbing complexes on the surface of the catalyst. The formation of this complex produces hydronium ion, which control desorption of CT from the surface to the bulk solution [33, 34]. In the absence of paths leading to its formation in the aqueous phase, CT might be undetectable using the high irradiation dosage (1.6 and 0.8MGY), even if it forms at the semiconductor–water interface, because it undergoes rapid photocatalytic degradation directly at the interface. Moreover, the irradiation dose can affect the transfer of the CT into bulk solution and consequently have a positive impact on the degradation reaction.

Conclusion

The following are the main conclusions that may be drawn from the results obtained: Fe doped TiO₂ system consists of nano-sized phases, the crystallite sizes of these phases are affected by irradiation with gamma rays . It is worth noting the effect of γ -irradiation on the improvement of the photo-catalytic activity and photo degradation of 2-chlorophenol. Only the high dose of γ -irradiation (**1.6MGy**) showed the highest photocatalytic activity, this increase in photocatalytic activity is could be related to the following reasons:

- The observed increase in their BET. Because, it has been reported that the main function of γ -irradiation of some catalytic solid systems took place via splitting of particles of the irradiated solids and fragmentation of catalyst's constituents.
- The observed increasing in the intensity of surface acidity , the amount of surface acid sites and acid sites strength can be attributed to the effect of γ -irradiation on creation new pores on the surface of the catalyst
- The enhancement of the activity of irradiated Fe/TiO₂ catalysts in comparison to non-irradiated one may be due to different content of FeTiO₃ (according XRD) and highly homogeneous dispersion of iron species on surface. Especially, the FeTiO₃ improve the photocatalytic activity of irradiated Fe/TiO₂ systems. Because FeTiO₃ has a good light absorbance and favorable photo-excited electron-hole separation characters.

References

1. Bzdon S.; J. Goralski; W. Maniukiewicz and J.Perkowski (2012) "Radiation-induced synthesis of Fe-doped TiO₂: Characterization and catalytic properties" Radiation Physics and Chemistry, 81, 322-330.
2. Adan C.; A. Bahamonde; M. Fernandez-Garcia and A. Martinez-Arias (2007) "Structure and Activity of Nanosized Iron-Doped Anatase TiO₂ Catalysts for Phenol Photocatalytic Degradation" Applied Catalysis B: Environmental, 72, 11-17.
3. Meire, M.; S. W. Verbruggen; S. Lenaerts; P. Lommens; P. Van Der Voort; I. Van Driessche (2016) " Microwave-assisted synthesis of mesoporous titania with increased crystallinity, specific surface area, and photocatalytic activity" .Journal of Materials Science, 51, 9822-9829.
4. Coronado J.M.; J. Soria; J.C. Conesa; R. Bellod; C. Adan; H. Yamaoka; V. Loddo and V. Augugliaro (2005) "Photocatalytic inactivation of Legionella Pneumophila and aerobic bacteria consortium in water over TiO₂/SiO₂ fibres in a continuous reactor" Topics in Catalysis, 35, 279 -286.

5. Leon Choreno A.; N. Portillo Velez; I. Hernandez Perez; R.Suarez Parra; M. May Lozano; L. Gonzalez Reyes; and R. Luna Paz (2013) "Effect of Ti content in the photocatalytic behavior of Fe/TiO₂-SiO₂ systems" *Revista Mexicana de Fisica*, 59 , 158-162.
6. Sangchay W. (2017) "Photocatalytic and antibacterial activity of Ag-doped TiO₂ nanoparticles" *Asia-Pacific Journal of Science and Technology*, 18, 731-738.
7. Alijani S.; M. Vaez and A. Z. Moghaddam (2014) "Photocatalytic Degradation of Acid Red Using TiO₂ Nanoparticles Immobilized on Alumina Foam" *International Journal of Environmental Science and Development*, 5, 104-107.
8. Arslan I.; L.A. Balcioglu and D.W. Bahnemann (2000) "Heterogeneous photocatalytic treatment of simulated dyehouse effluents using novel TiO₂-photocatalysts", *Applied Catalysis B* 26, 193-206.
9. Nalbandian, M. J.; K. E Greenstein; D. Shuai; M. Zhang; Y. H. Choa; G. F. Parkin; D. M Cwiertny (2015) "Tailored synthesis of photoactive TiO₂ nanofibers and Au/TiO₂ nanofiber composites: structure and reactivity optimization for water treatment applications" *Environmental science & technology*, 49, 1654-1663..
10. Hincapié P. M.; G. Peñuela; M. I. Maldonado; O. Malato; P. Fernández-Ibáñez; I. Oller; W. Gernjak and S. Malato (2006) "Degradation of pesticides in water using solar advanced oxidation processes" *Applied Catalysis B: Environmental*, 64, 272-281.
11. Li Y., S. Peng; F. Jiang; G. Lu and S. Li (2007)"Effect of doping TiO₂ with alkaline earth metal ions on its photocatalytic activity" *Journal Of The Serbian Chemical Society*, 72 , 393-402.
12. Gabriela G; C.Garcia; A. M. Hernandez and J. J.Becerril (2012) "Use of TiO₂ as Catalyst in Degradation Induced with γ - Radiation of Methylene Blue" *journal of the chemical Society of Pakistan*, 34, 533-535.
13. Sharma S. L. and T. K. Maity (2011) "Effect of gamma radiation on electrical and optical properties of (TeO₂) (In₂O₃) thin films" *The Bulletin of Materials Science*, 34, 61-69.
14. El-Shobaky G.A.; M.M. Doheim; A.M. Ghozza and H.A. El-Boohy (2002) "Catalytic conversion of ethanol over Co₃O₄/MgO system treated with γ -irradiation" *Materials Letters*, 57, 525- 531.
15. El-Shobaky G. A.; M. M. Doheim, and A. M. Ghozza (2004)"Hydrocracking of cumene over Ni/ Al₂O₃ as influenced by CeO₂ doping and γ - Irradiation *Radiation Physics and Chemistry* 69 ,31-37.
16. Doheim M.M.; H.A. El-Boohy and G.A. El-Shobaky (2001) "Catalytic Conversion of Ethanol and Iso propanol on γ -Irradiated Co₃O₄/Al₂O₃ solids" *Adsorption Science & Technology*, 19, 635-641.
17. Ye F.X.; T. Tsumura; K. Nakata and A. Ohmori (2008) "Dependence of photocatalytic activity on the compositions and photo-absorption of functional TiO₂-Fe₃O₄ coatings deposited by plasma spray" *Materials Science and Engineering*, 148, 154-161.
18. Cullity B.D. (1978) "Elements of X-Ray Diffraction", 2nd Ed, Addison- Wesley, MA, USA, 102.
19. El-Molla S. A.; S. A. Ismail and M. M. Ibrahim (2011) "Effects of γ -Irradiation and Ageing on Surface and Catalytic Properties of Nano-sized CuO/MgO System" *Journal of the Mexican Chemical Society*, 3, 55-56.
20. Vijayalakshmi R; and V; Rajendran (2012)"Synthesis and characterization of nano-TiO₂ via different methods" *Archives of Applied Science Research*, 2, 1183-1190.
21. Balachandran U; and N.G. Eror (1982) "Raman spectra of titanium dioxide" *Journal of Solid State Chemistry* 42, 276- 282.
22. Ganesh I.; P. P. Kumar; A.K. Gupta; P. S.C. Sekhar; K. Radha, G. Padmanabham and G. Sundararajan, (2012) "Preparation and characterization of Fe-doped TiO₂ powders for solar light response and photocatalytic applications" *Processing and Application of Ceramics*, 6, 21-36.
23. El-Shobaky H.G.; A.S. Ahmed and N.R. Radwan (2006) "Effect of γ -irradiation and ZnO-doping of CuO/TiO₂ system on its catalytic activity in ethanol and isopropanol conversion *Colloids and Surfaces A: Physicochem. Eng. Aspects*, 274, 138–144.
24. Samantaray S. K. and K. Parida (2001) Effect of phosphate ion on the textural and catalytic activity of titania-silica mixed oxide, *Applied Catalysis A: General*. 220, 9–20.
25. Chen F.; J. Zhao and H. Hidaka (2003) "Adsorption factor and photocatalytic degradation of dye-constituent aromatics on the surface of TiO₂ in the presence of phosphate anion" *Research on Chemical Intermediates* 29, 733-748.
26. Tsai S. and S. Cheng; (1997) "Effect of TiO₂ crystalline structure in photocatalytic degradation on of phenolic contaminants" *Catalysis Today*, 33, 227-237.
27. Hsien V.H.; C.-F.Chang; Y.H.Chen; and S.Cheng (2001) "Photodegradation of aromatic pollutants in water over TiO₂ supported on molecular sieves". *Applied Catalysis B: Environmental*, 31, 241-245.
28. Abdel-Aal A.A.; S.A. Mahmoud and A.K. Aboul-Gheit (2009) "Sol-Gel and Thermally Evaporated Nanostructured Thin ZnO Films for Photocatalytic Degradation of Trichlorophenol" *Nanoscale Research Letters*, 4, 627-634.
29. Cho Y.M.; W.Y. Choi; C.H. Lee, T.H. Hyeon and H.I. Lee (2001) "Visible light-induced degradation of carbon tetrachloride on dye-sensitized TiO₂" *Environmental Science & Technology*, 35, 966-970.

30. Xu N.; Z. Shi; Y. Fan; J. Shi and M.Z.C.Hu (1999) "Effects of particle size of TiO₂ on photocatalytic degradation of methylene blue in aqueous suspensions" *Industrial and Engineering Chemistry*, 38, 373-379.
31. Gerischer H. (1995) "Photocatalysis in aqueous solution with small TiO₂ particles and the dependence of the quantum yield on particle size and light intensity" *Electrochimica Acta*, 40, 1277-1281.
32. Ilisz I.; A. Dombi; K. Mogyorosi; A. Farkas and I. Dekany (2002) "Removal of 2-chlorophenol from water by adsorption combined with TiO₂ photocatalysis" *Applied Catalysis B: Environmental*, 39, 247-256.
33. Jankovic I.A., Z.V. Saponjic, E.S. Dzunuzovic and J.M. Nedeljkovic (2010) "New Hybrid Properties of TiO₂ Nanoparticles Surface Modified With Catecholate Type Ligands " *Nanoscale Research Letters*, 5, 81-88.
34. Betiha M. A.; S. A. Mahmoud; M. F. Menoufy and A. M. Al-Sabagh (2011) "One-pot template synthesis of Ti–Al containing mesoporous silicas and their application as potential photocatalytic degradation of chlorophenols" *Applied Catalysis B: Environmental*, 107, 316– 326.
35. Puma G.L; and P.L. Yue (2002) "Effect of radiation wavelength on the rate of photocatalytic oxidation of organic pollutants" *Industrial and Engineering Chemistry Research*, 41, 5594- 5600.